Water Research 255 (2024) 121398

Contents lists available at ScienceDirect

Water Research

journal homepage: www.elsevier.com/locate/watres

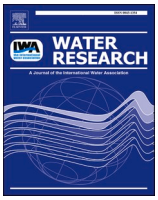

Numerical modelling of surface aeration and N_2O emission in biological water resource recovery

Yuge Qiu [a,*], Sara Ekström [b], Borja Valverde-Pérez [b], Barth F. Smets [b], Javier Climent [c], Carlos Domingo-Félez [b], Raúl Martínez Cuenca [c], Benedek G. Plósz [a,d]

[a] Department of Chemical Engineering, University of Bath, Claverton Down, Bath BA2 7AY, UK
[b] Department of Environmental Engineering, Technical University of Denmark, Bygningstorvet, Building 115, 2800 Kgs., Lyngby, Denmark
[c] Department of Mechanical Engineering and Construction, Universitat Jaume I, Av. Vicent Sos Baynat, s/n 12071 Castellón (Spain)
[d] SWING – Department of Built Environment, Oslo Metropolitan University, St Olavs plass 0130, Oslo, Norway

ARTICLE INFO

Keywords:
Biological water resource recovery
Oxygen and N_2O gas mass-transfer
Surface aeration
Computational fluid dynamics
Calibration of single- and two-phase models
Factor screening using design of experiment

ABSTRACT

Biokinetic modelling of N_2O production and emission has been extensively studied in the past fifteen years. In contrast, the physical-chemical hydrodynamics of activated sludge reactor design and operation, and their impact on N_2O emission, is less well understood. This study addresses knowledge gaps related to the systematic identification and calibration of computational fluid dynamic (CFD) simulation models. Additionally, factors influencing reliable prediction of aeration and N_2O emission in surface aerated oxidation ditch-type reactor types are evaluated. The calibrated model accurately predicts liquid sensor measurements obtained in the Lynetten Water Resource Recovery Facility (WRRF), Denmark. Results highlight the equal importance of design and operational boundary conditions, alongside biokinetic parameters, in predicting N_2O emission. Insights into the limitations of calibrating gas mass-transfer processes in two-phase CFD models of surface aeration systems are evaluated.

1. Introduction

Global warming and the climate emergency constitute the most critical global sustainability challenges. Policy responses to climate change impacts comprise mitigation measures, addressing the causes by reducing anthropogenic greenhouse gas emissions. The reduction of greenhouse gas emissions in the form of N_2O, – representing the majority of the carbon footprint of WRRF systems (Kampschreur et al., 2009; Ribera-Guardia et al., 2019)– requires the development of effective reactor design and operational solutions. Whilst, ample literature evidence exists on the metabolic pathways, stoichiometry and biokinetics of microbial conversion of nitrogenous chemicals that can lead to N_2O release from biological treatment processes (Kampschreur et al., 2009, 2008), it is less well understood how bioreactor design and operational conditions – and the interplay between bioconversion and transport processes in full-scale reactor systems – can influence overall N_2O emission – the main focal area of the present study. This is extremely important, because the spatially and temporarily changing reactor environments can significantly impact the removal of microbially produced N_2O in, for instance, surface aerated oxidation ditch activated sludge bioreactors. Gaining a better insight into such highly-coupled biokinetic-transport phenomena is key to develop the next-generation WRRF process design and operation. Regarding biokinetic modelling of N_2O, there are single- and two-pathway models developed that include nitrifier nitrification (NN) and/or denitrification (ND) only (Ni et al., 2013; 2014; Pocquet et al., 2016). In comparison, the NDHA process model (Domingo-Félez et al., 2016), includes nitrifier nitrification (N), nitrifier denitrification (D), heterotrophic denitrification (H) and abiotic N_2O conversion processes (A). That is, the NDHA model includes not only NN and ND pathways, but also heterotrophic denitrification (HD) and abiotic N_2O production pathways that is an advantage when it comes to full-scale WRRF simulations – a key argument to implement it in our CFD simulation model.

In-reactor oxygen availability is a key factor influencing N_2O production. There are two common types of aeration systems in oxidation ditch modelling: compressed-air fine-bubble and mechanical surface aeration (Tchobanoglous et al., 2003). Despite their lower oxygen transfer efficiency, compared to fine-bubble aeration (Al-Ahmady, 2006; Gehring and Lindam, 2013; Guanghao et al., 2020), surface-aerated activated sludge reactors (SASR) found widespread implementations, e.g., in France and Denmark. This is because they are relatively simple

* Corresponding author.
E-mail address: yq306@bath.ac.uk (Y. Qiu).

https://doi.org/10.1016/j.watres.2024.121398
Received 28 November 2023; Received in revised form 15 February 2024; Accepted 27 February 2024
Available online 29 February 2024

Nomenclature

Abbreviation

3D	Three-dimensional
BSD	Bubble size distribution
CFD	Computational fluid dynamic
DO	Dissolved oxygen
GCI	Grid convergence index
OTR	Oxygen transfer rate
PBM	Population balance model
SASR	Surface-aerated activated sludge reactors
SST	Shear stress transport model
WRRF	Wastewater resource recovery facility

Symbols

a	Alpha factor [-]
b	Beta factor [-]
b_i	Normalised sensitivity index [-]
η_{NOR}	Reduction factor for NO reduction [-]
μ	Dynamic viscosity [N s m^{-2}]
μ_{NOB}	Maximum aerobic nitrite-oxidizing (NOB) growth [h^{-1}]
$\mu_{AOB,\ HAO}$	Maximum growth rate for hydroxylamine (NH_2OH) oxidation [h^{-1}]
$\mu_{AOB,\ AMO}$	Maximum growth rate for ammonia (NH_3) oxidation [h^{-1}]
ρ	Density [kg m^{-3}]
τ_{ij}	Reynolds stress [-]
ω_{rotor}	Rotor speed [rpm]
D_φ	Molecular diffusivity [m^2 s^{-1}]
D_{rotor}	Blades diameter [m]
F_S	Safety factor for GCI calculation [-]
$K_L a_{N2O}$	Overall liquid phase mass transfer coefficient of N_2O [h^{-1}]
$K_L a_{O2,clean}$	Overall liquid phase mass transfer coefficient of O_2 in clean water [h^{-1}]
L_{rotor}	Rotor axis length [m]
MW_i	Molar mass of component i [kg mol^{-1}]
M_{rotor}	Rotor momentum source [kg m s^{-1}]
N_{rotor}	Rotor power number [-]
Sc	Schmidt number [-]
S_i	Liquid concentration of component i [mg L^{-1}]
S_O*	Saturation liquid concentration of oxygen [mg L^{-1}]
T	Temperature [°C]
U_i	Velocity field components [m s^{-1}]
V_{rotor}	Volume of rotor [m^3]
X_{tot}	Total biomass concentration in reactor [mg L^{-1}]
b_i	Sensitivity index [-]
$e_{i(i-1)}$	Relative error between test i and i-1 [-]
g	Gravity acceleration [m s^{-2}]
h_{rotor}	Rotor submergence [m]
$r_{i(i-1)}$	Grid refinement ratio between mesh i and i-1 [-]
v_i	Fluid velocity at position i [m s^{-1}]

and cheap to install, have low maintenance costs and are easy to control via variable rotor speed and submergence depth (Cumby, 1987; Guanghao et al., 2020; Mueller et al., 2002; Stenstrom and Gilbert, 1981).

CFD simulation models can be used to predict and optimize the performance of complex reactor operations such as SASR (Karpinska and Bridgeman, 2016). Most CFD studies on aeration systems and aerated reactors focus on bubble diffusers or air spargers (Le Moullec et al., 2010; Niño et al., 2020; Zaburko et al., 2020). There is limited knowledge on surface aerator CFD modelling (Karpinska and Bridgeman, 2016), both in terms of their fluid dynamics and aeration gas transfer behaviour – significant knowledge gaps the present study aims to cover. To this end, the first aspect is to introduce an equivalent momentum source term into the hydrodynamic equations. The second aspect of model development entails the development of a mechanistic multiphase model that requires two-phase data on the spatial distribution of bubbles introduced by the surface aerating rotors and a detailed characterization of the bubble sizes. The latter – representing a major knowledge gap – is beyond the scope of the present study – partly, due to its inherent complexity. Instead, this study evaluates the approach of using (A) uniform spatial distribution of the generated bubbles limited to the region occupied by the rotors and (B) bubble-size population balance modelling previously used for aeration diffusers (e.g., Climent et al., 2019)

Mesh generation – critical for following good practice in CFD modelling (Roache, 1998; Wilcox., 1998) – can follow unstructured and structured approaches. Unstructured mesh is normally built for complex geometry of e.g., corners and sharp edges in reactors. Compared to structured mesh, the generation of unstructured mesh is quicker; however, it comes with an increased computational memory requirement for storing a higher number of elements, which in turn increases the computational time (Sack and Urrutia, 2008). Implementing structured mesh can result in higher mesh quality as a result of higher degree of control over e.g., inflation layers, number of elements and nodes (Wicklein et al., 2016).

In this study, the shear stress transport (SST) model is implemented for the turbulence description. Compared to other turbulence models, the SST turbulence model combines the features of $k-\varepsilon$ and $k-\omega$ turbulence models to simulate free stream and wall regions, respectively; it's also a simpler tool, and as such, it can also reduce computational time as well as it provides relatively accurate results (Menter, 1993; Wilcox., 1998, 2009). As for predicting N_2O greenhouse gas emission from activated sludge processes, most studies in literature focus on discriminating biokinetic model parameters (Ni et al., 2013; Ni et al., 2014; Pocquet et al., 2016; Domingo-Félez et al., 2017). In turn, there is a significant knowledge gap as to how uncertainties from design and operational parameters propagate to simulation outputs obtained with combined biokinetic-transport models.

To reduce model complexity, whilst maintaining high predictive accuracy, complex hydrodynamic simulation models can be converted into simple distributed (1-dimensional) models using data-driven models (Guyonvarch et al., 2015; 2020; Schneider et al., 2022). In this study, statistical meta-models are identified for gas-liquid mass transfer in SASR using steady-state CFD simulation results.

CFD simulation models to predict the behaviour of aerated reactor systems are widely implemented. Whilst for fine-bubble aeration systems, this approach can result in accurate model predictions – thanks to the wealth of related literature evidence on the underlying physical phenomena – this is not the case for surface aerated systems. Notably, we show here that, due to the lack of robust understanding of bubble structure and terminal velocity in surface aeration, the practice of substituting related fine-bubble aeration data to calibrate surface aeration models (e.g., Matko et al., 2021) can lead to erroneous solutions. To this end, our results indicate the need for improved understanding of the spatial variability of gas mass transfer behaviour, downstream to the surface aeration rotor, which is found to be key to reliably predict both DO and N_2O mass transfer.

Following the principles of statistically interpreted CFD, the regression meta-models identified for surface aeration here – using 3-D CFD simulation results – are proposed to be used to dynamically calibrate gas mass-transfer models in WRRF plant-wide simulations.

The main objectives of this paper focus on answering the hypothesis tests of (A) systematic numerical model identification and calibration for

reliable prediction of dissolved oxygen and N_2O gas mass-transfer processes in surface aerated reactors; (B) evaluating calibration methods for single- and two-phase 3-D CFD simulations to discriminate numerical simulation model structures; and (C) analysis of parameter sensitivity to predict dissolved oxygen and N_2O greenhouse gas emission simulation outputs as well as to develop good modelling practices.

2. Calibration of CFD models of surface aerated reactor systems

For the surface aeration systems, CFD simulation model calibration involves a number of parameters, some of which are specific to single- and two-phase simulations (Fig. 1). Here we present a comprehensive overview on the calibration methods for surface aerations – presently a considerable research gap (Amaral et al., 2017).

2.1. Common (single- & two-phase) parameters and single-phase model parameters

To calibrate the total oxygen transfer rate (TOTR) [kg O_2 h^{-1}], pertinent information on rotor type is typically provided by manufacturers as a function of rotor speed and submergence. TOTR through surface aeration can be calibrated as a function of rotor operational speed (ω_{rotor} [rpm]), rotor submergence, h_{rotor} [m] and rotor length [m] (Fig. 2), i.e.

$$TOTR = \left[(0.793 \times \omega_{rotor} - 26.94) \times h_{rotor} + 15.14e^{-0.041\omega_{rotor}}\right] \times L_{rotor} \quad (1)$$

We note that Eq. (1) is only valid within the range of rotor speed, spanning from 55 to 83 rpm and the range of rotor submergence, from 0.1 to 0.25 m. For model calibration, the rotor submergence of 0.2 m and rotor speed of 55 rpm were used.

The *a* factor is the ratio of the gas-liquid gas mass-transfer coefficient measured in wastewater (K_La_{WW}) to that obtained in clean water tests ($K_La_{O2,clean}$), i.e., $k_La_{ww}/k_La_{O2,clean}$ (Rosso and Stenstrom, 2014, 2006; Stenstrom and Gilbert, 1981; Tewari and Bewtra, 1982); its value can vary as a function of the physical and operational boundaries of the aeration system and wastewater characteristics (Bencsik et al., 2022). Here, we present *a* factor calibration method using full-scale hood measurements and CFD simulation results (Fig. 8) that is described as follows.

Values of $K_La_{O2,clean}$ are estimated at the five monitoring points using CFD simulation results (Fig. 7b). These results – combined with K_La_{N2O} data (measured using liquid- and gas-phase sensor data, Eq. 12.) – are substituted in the regression equation (Eq. (2)), and are then used to approximate a single a value using a one-parameter estimation method (SigmaPlot, 12.1). To estimate the spatially varying values of $K_La_{O2,clean}$, transient-to-steady-state simulations – in the absence of active biomass – were run to simulate oxygen concentration time-series profiles at different spatial monitoring points (Fig. S2). Values of $K_La_{O2,clean}$ were estimated using the dissolved oxygen concentration data obtained in fifteen different spatial monitoring points downstream to the surface aerator (Fig. 4). That is, in addition to the five sensor monitoring points – in the real system – located close to liquid surface (Fig 4a), two additional vertical monitoring points were defined – in the CFD simulation domain – for each horizontal location in the CFD domain at 0.5- and 1.0-m depths (Fig. 4b). The $K_La_{O2,clean}$ field is computed as a function of the distance to the rotor using correlation equations for the $K_La_{O2,clean}$ values obtained (Fig. 4). Separate correlation equations are established for the surface layer and for the layer underneath, i.e., the sub-surface layer (Fig. 7c and d). Laboratory-scale measured data (reported by Domingo-Félez et al., 2014) – obtained in off-site batch experiments – are used here to infer a new correlation equation for K_La_{N2O} and $K_La_{O2,clean}$ as

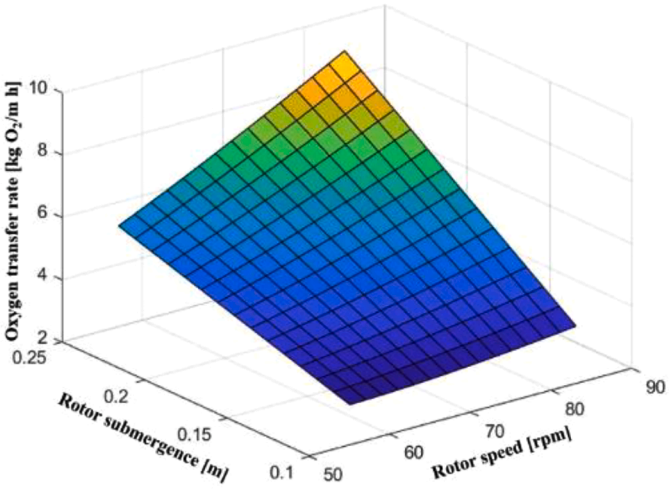

Fig. 2. Length normalised oxygen transfer rate (OTR, kg m-1h-1) – 3-D plane for surface aerator OTR defined as a function of rotor submergence and rotor speed, Eq. 1 (Dage, 2017).

$$K_La_{N2O} = \left[0.14 \cdot \ln\left(K_La_{O2,\ clean} \cdot \alpha\right) + 1.17\right] K_La_{O2,\ clean} \cdot \alpha \quad (2)$$

where $K_La_{O2,clean}$ and K_La_{N2O} [min^{-1}] are gas-liquid mass transfer coefficient for oxygen in clean water and for N_2O in wastewater, respectively. Subsequently, the a factor – considered as an average value for the entire reactor – was approximated by fitting Eq. (2) to K_La_{N2O} data. To predict the in-reactor K_La_{N2O} field, Eq. (2) is implemented in the CFD simulation model for both the reference system (Lynetten WRRF) and those included in the factorial screening study.

For oxygen saturation concentration (So^*), a temperature dependence correlation (Eq.3) is implemented (Plósz et al., 2003), i.e.,

$$So^* = \left(-0.00008T^3 + 0.008T^2 - 0.4102T + 14.65\right)\beta \quad (3)$$

where T is the fluid temperature (°C). The *b* factor is the ratio between

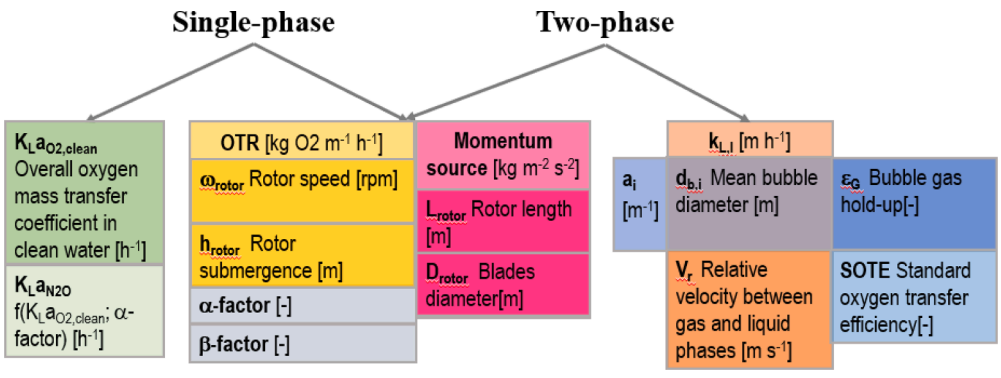

Fig. 1. Calibrated Parameters for single- and two-phase CFD simulation models.

DO concentration in wastewater and that in clean water (Tewari and Bewtra, 1982). In this study, a constant value of was used (Plósz et al., 2003; Tewari and Bewtra, 1982).

The surface aeration rotors are modelled by following the so-called momentum source approach (Huang et al., 2013; Murthy and Jayanti, 2002). Therefore, the geometry of blades of the impellers are not included explicitly in the computational domain. Instead, the overall effect of the rotors on the flow is approximated by a momentum source that is limited to act within the cylindrical region that is occupied by the rotor when it rotates. Accordingly, the volume of this region is given as

$$V_{rotor} = \frac{\pi}{4} L_{rotor} D_{rotor}^2, \tag{4}$$

where L_{rotor} denotes the rotor axis length [m]. D_{rotor} represents the blades diameter ($D_{rotor} = 2R_{rotor}$) in [m]. The momentum source of every rotor (M_{rotor}) is introduced as:

$$M_{rotor} = \frac{P_{rotor}}{2\pi\ \omega_{rotor} R_{rotor} V_{rotor}}, \tag{5}$$

where P_{rotor} stands for the rotor power calculated as

$$P_{rotor} = N_{rotor}\ \rho\ \omega_{rotor}^3 D_{rotor}^5 \tag{6}$$

ω_{rotor} represents the rotor angular speed [rpm]. N_{rotor} is the rotor power number that is related to the propeller efficiency. The value of N_{rotor} is assumed to be 0.25 (Hemrajani and Tatterson, 2004).

2.2. Two-phase model parameters

Two-phase CFD simulation models of aerated reactors can be used to account for bubble characteristics, thus improving the prediction aeration tank performance (Climent et al., 2019; Guo et al., 2020; Karpinska and Bridgeman, 2016). To predict gas mass-transfer in two-phase models, the three key sub-models to calibrate include the specific interfacial area for gas-liquid mass transfer a_i [m^{-1}]; the liquid-phase mass transfer coefficient k_L [m h^{-1}]; and surface aerator boundary condition separately (Karpinska et al., 2016; Guo et al., 2020).

In the two-phase simulation model, the second phase is described according to the Eulerian-Eulerian Two-Fluid model (Climent et al., 2019) using the following correlations for the interfacial forces:

- Ishii-Zuber for the drag coefficient.
- Tomiyama for the lift coefficient.
- Favre averaged coefficient (0.2) for the turbulent dispersion.
- Sato model for bubble induced turbulence.

The population balance of air bubbles is modelled using the MUSIG method, describing bubble coalescence with Prince & Blanch model (Prince and Blanch, 1990) and bubble break-up with Luo and Svendsen (1996). The settings of bubble group sizes ensures that the coalescence does not lead to a saturation of the bigger size groups. The following bubble-size groups were implemented in our CFD simulation model: 0.5 mm, 1 mm, 2 mm, 3 mm, 5 mm, 8 mm, 12 mm and 20 mm. The mass transfer terms for N_2O stripping and O_2 aeration are implemented using interfacial terms as

$$S_{O2,\ liquid} = k_{L,O2} a_i \alpha \left(C_{O2,gas} / H_{O2} - C_{O2,liq}\right) \tag{7}$$

$$S_{N2O,\ liquid} = -k_{L,N2O} a_i \left(C_{N2O,gas} / H_{N2O} - C_{N2O,liq}\right) \tag{8}$$

Regarding the mass transfer coefficients, K_L, its value can be estimated in two-phase CFD models with correlation equations using the dimensionless Schmidt number (Sc), friction velocity, molecular diffusivity of the liquid phase (Deacon, 1977; Gostelow et al., 2001; Hibiki and Ishii, 2011; Mackay and Yeun, 1983; Prata et al., 2018; US EPA, 2001, 1994), i.e.,

$$k_{L,i} = 2\sqrt{\frac{D_{L,i} V_r}{\pi d_b}} \tag{9}$$

where $D_{L,i}$ is the diffusion coefficient for species i [$m^2\ s^{-1}$], V_r the relative speed between the phases [m s^{-1}] and d_b the mean bubble size [m]. In this way, V_r is calculated using the code from the velocity vectors of the gas ($\vec{V}_{gas}$) and liquid phases ($\vec{V}_{liquid}$) as $V_r = \left|\vec{V}_{gas} - \vec{V}_{liquid}\right|$. The interfacial area concentration, a_i, [m^{-1}] was calculated from the gas hold up, ε_G [-], and the mean bubble size, i.e.

$$a_i = \frac{6\varepsilon_G}{d_b}. \tag{10}$$

The corresponding source terms were added to the gas phase to ensure mass conservation of the N_2O and O_2.

It is difficult-to-impossible to measure the oxygen mass transferred from air into liquid around the aerator using surface aeration. Therefore, we propose to model aeration efficiency through bubble generation intensity by the rotors, modelled using the mass source term (limited to the regions that contain the rotors) as

$$S_{bubble} = TOTR/SOTE \tag{11}$$

In this equation, OTR stands for the Total Oxygen Transfer Rate as given by correlation in Eq. (1), and SOTE denotes a theoretical Standard Oxygen Transfer Efficiency in wastewater. SOTE is used here as a calibration parameter for the surface rotors by approximating the measured oxygen levels.

3. Materials and methods

3.1. Sampling and data collection

For model calibration, measured data were collected in the Lynetten full-scale WRRF, Denmark. Online sensors (Unisense, Demark) were installed in the oxidation ditch (spatial points shown in Fig. 4, Fig. S2), including four N_2O liquid-phase sensors and two dissolved oxygen (DO) sensors.

Moreover, a N_2O gas-phase sensor was installed in a gas hood (Fig. 3) collecting gas samples in the headspace of the reactor to quantify the N_2O gas stripping mass transfer coefficient, $K_L a_{N2O}$, as

$$K_L a_{N2O} = \frac{\frac{q_{air} \times p_{N2O}}{RT} \times MW_{N2O}}{V_R \times \left(S_{N2O} - S_{N2O}^*\right)}, \tag{12}$$

where the q_{air} is the volumetric flow rate of air [L h^{-1}], p_{N2O} is the partial pressure of N_2O [atm], MW_{N2O} is the molar mass of N_2O [44 g mol^{-1}], V_R is the volume of the reactor (control volume) [L], S_{N2O} and S_{N2O}^* are the liquid concentration and saturation concentration of N_2O, respectively [g L^{-1}], R is the gas constant [atm L mol^{-1} K^{-1}] and T is the temperature [K]. Fig. 3 shows the details of the gas collection hood. Under the hood, there are gas sensors, which measure the partial pressure of N_2O, and liquid sensors, which measure the N_2O concentration in the liquid phase. More information on measured data including flow rate (Fig. S6), influent and effluent concentrations are shown in SI (Fig. S7–8). Additionally, sensors used to monitor chemicals during the sampling campaign, include Total Suspended Solids, TSS (Solitax SC, Hach); NH_4-N (Amtax SC, Hach); NO_3-N (Nitratax SC, Hach); PO_4-P (Phosphax SC, Hach). Offline laboratory measurements were done – e.g., to calibrate sensors - according to (APHA, 1999).

3.2. Biokinetic model

The NDHA process model (Domingo-Félez and Smets, 2016; 2020) is implemented in the CFD simulation model to predict the biokinetics of nitrogen removal, including N_2O production and consumption. The NDHA model, a state-of-art biokinetic model, accounts for N_2O

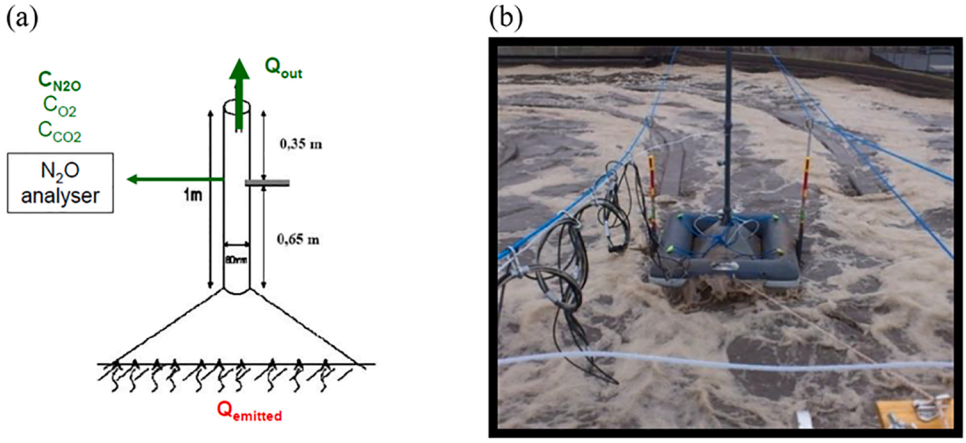

Fig. 3. (a) Schematic drawing and (b) picture from Lynetten plant of N2O hood. The gas-collection hood was moved between five different sampling points downstream to the surface aeration rotor (Fig. S1).

production via nitrifier nitrification (N), nitrifier denitrification (D), heterotrophic denitrification (H) and abiotic reactions (A). One of the major advantages of NDHA is the systematic calibration protocol and the practical identifiability of the model structure (Domingo-Félez et al., 2017), as compared to other process models (Ni et al., 2013; Ni et al., 2014; Pocquet et al., 2016). All the parameters are shown in the SI (Table S1).

3.3. Mesh generation (GCI)

The mesh generation was carried out in two different ways. On the one hand, the mesh was generated using Ansys CFX's in-built generation tool, hereby referred to as the unrefined mesh (Fig. S4). Second, a systematic mesh refinement to mesh quality comparison were carried out (Fig. 4) using the Grid Convergence Index (GCI) test (Baker et al., 2020). The equations to calculate GCI values are shown in the SI.

3.4. Numerical methods

The CFD simulations rely on the Reynolds-Averaged Navier–Stokes (RANS) equation for incompressible-Newtonian flows. For isothermal flows, the flow dynamics obeys the following conservation equations for mass and momentum:

$$\frac{\partial \rho}{\partial t} + \rho \frac{\partial U_j}{\partial x_j} = 0 \tag{13}$$

$$\rho \frac{\partial U_i}{\partial t} + \rho \frac{\partial}{\partial x_j}\left(U_i U_j\right) = -\frac{\partial p}{\partial x_i} - \frac{2}{3}\mu \frac{\partial U_j}{\partial x_j} + \mu \frac{\partial}{\partial x_j}\left(\frac{\partial U_i}{\partial x_j} + \frac{\partial U_j}{\partial x_i}\right) - \frac{\partial \tau_{ij}}{\partial x_j} + \rho g_i + M_i. \tag{14}$$

These equations relate fluid properties such as dynamic viscosity (μ [Pa s]) and density (ρ [kg m^{-3}]) with the mean pressure (p [Pa]) and velocity field components (U_i [m s^{-1}]), including the turbulence effects through the Reynolds stresses (τ_{ij}). External forces such as gravity vector components (g_i) and the volumetric momentum source components (M_i) are also included.

For the SST turbulence model, the Reynolds stresses are given in terms of turbulent viscosity (μ_t) and the mean velocity gradients as

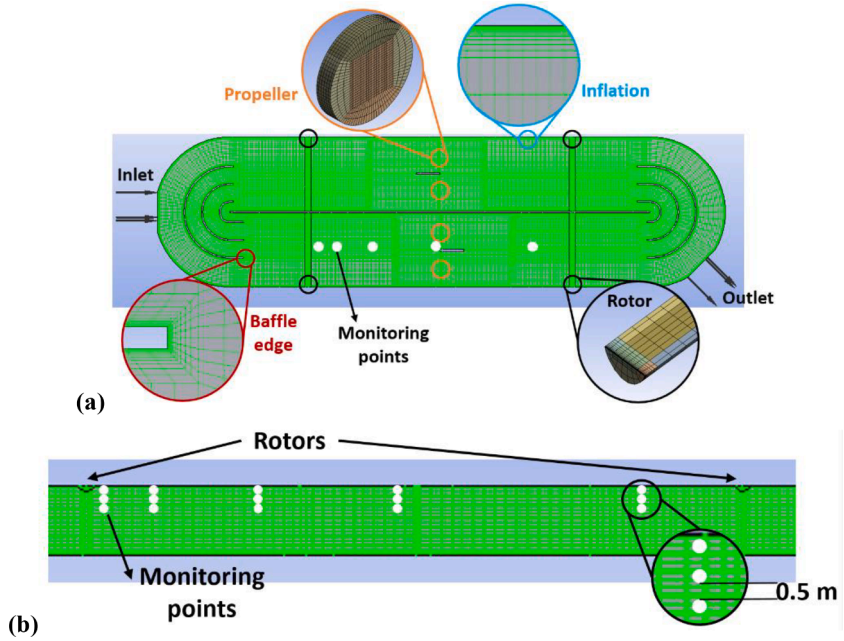

Fig. 4. The design layout and mesh of the oxidation ditch in Lynetten WRRF - (a) top view and (b) side section view.

$$\tau_{ij} = \mu_t \frac{\partial}{\partial x_j}\left(\frac{\partial U_i}{\partial x_j} + \frac{\partial U_j}{\partial x_i}\right). \quad (15)$$

For more details on the SST model implementation and the use of wall functions, the reader is referred to the ANSYS CFX 19.1 help function. The implementation of the biokinetic model implementation was done by the addition of a conversion term to the overall mass-balance eachation to compute the dynamics of the volumetric concentration of each variable, φ_k, as

$$\rho \frac{\partial \varphi_k}{\partial t} + \rho \frac{\partial}{\partial x_j}\left(U_j\ \varphi_k\right) = \frac{\partial}{\partial x_j}\left[\left(\rho D_{\varphi_k} + \frac{\mu_t}{Sc_t}\right)\frac{\partial \varphi_k}{\partial x_j}\right] + S_{\varphi_k} \quad (16)$$

being D_{φ_k} the molecular diffusivity for the k^{th} variable and Sc_t the turbulent Schmidt number, that is set to 0.9 (Tominaga and Stathopoulos, 2007). The biokinetic reaction rate terms are included in the volumetric source terms, S_{φ_k}.

3.5. CFD simulations

In this study, a 3-D CFD simulation model is first developed using the design and operational boundary conditions as well as experimental input data obtained in the Lynetten WRRF full-scale plant, employing an oxidation ditch-type reactor (Copenhagen, Denmark). All simulations were carried out using the software CFX-ANSYS®, Release R2 (Ansys, USA). Parameters values used to calibrate the model are shown in Table S1. The initial conditions are set according to Table S2.

The liquid temperature is fixed at 16.75 °C, which corresponds to that measured in the liquid phase during the onsite sampling campaign (Fig. S8). The pressure of the reactor head-space is set to 101.3 kPa. The boundary condition for the ditch wall was the no-slip condition and for the surface of the reactor, free-slip boundary condition was chosen. With the high-performance computing (HPC) system with the total memory of 15.8 TBs, the computational time for one simulation is around 4 to 5 h.

3.6. 2-level factorial screening study

A 2-level fractional factorial design was carried out using the maximum and minimum values (Table S3) for each parameter. The selected parameters include 3 different aspects: operating parameters, design parameters and biokinetic parameters, thereby resulting in 16 different meshes (Table S4).

To assess the relative sensitivity of selected CFD simulation outputs to design and operational boundary conditions, local sensitivity indices were calculated using linear polynomial regression equation (Guyonvarch et al., 2015; 2020). The regression plane (Y) is defined as

$$Y = b_0 + \sum b_i f_i \quad (17)$$

where f_i denotes the design and operational factors, b_i is the respective sensitivity indices, and b_0 represents the intercept value. To create sensitivity ranking for selected outputs, the normalized sensitivity indices (β_i) are calculated as:

$$\beta_i = b_i / b_0 \quad (18)$$

where the normalized sensitivity indices (β_i) are plotted for the selected simulation outputs. Besides K_La for oxygen, the simulation outputs include the N_2O emission factor calculated as (ICF, 2019):

$$N_2O\ emission\ factor = \frac{N_2O\ emitted\ (kg)}{Total\ N\ in\ (kg)} \times 100\% \quad (19)$$

Furthermore, the standardised regression polynomials (Eq. (17)) are converted into regression meta-models, representing so-called statistically interpreted meta-models (iCFD, Guyonvarch et al., 2015). These meta-models are then used to calibrate the CFD model in terms of $K_La_{O2,Clean}$ and to predict N_2O emission in WRRF plant wide models.

4. Results and discussion

4.1. Two-phase CFD simulation results and model discrimination

Here, we demonstrate the use of the calibration method to predict gas mass-transfer using surface aeration. Scenario simulations with a range of theoretical SOTE value are carried out using an optimised mesh (GCI=0.37; Table S5; Fig. S3; $i = 2$ in Table S6). Results obtained show that, using the two-phase CFD simulation model, accurate prediction is only achievable for dissolved oxygen concentration but not for both DO and N_2O (Fig. 5a).

The optimal SOTE value (1.5 %) – evaluated at a level that resulted in close agreement between the measured and simulated DO concentrations – (Fig. 5a and b) show that the surface aerator submergence can be related to that for fine-bubble aeration. This suggests that aerator submergence can serve as an effective measure to estimate values of SOTE using both surface and fine-bubble aeration – see correlation equation (Fig. 5b). Simulation results – obtained using SOTE=1.5 % (Fig. 6a) – indicate considerable spatial variability in surface DO concentrations with very low values close to the outer reactor wall.

Reactor volumes with low-DO can effectively create zones with enhanced biokinetic N_2O production and emission (Fig. 6b) – impacts that can be reduced by (A) installing baffles between the surface aerators; and (B) optimising the physical geometry of baffles (e.g., Huang et al., 2015; Teshome, 2020).

Whilst, these results are significant, to address the hypothesis tests of this paper, the two-phase CFD simulation model is found to be unfit for purpose. That is, despite the relatively high number of model parameters, successful model calibration is only feasible for DO and not for both DO and N_2O using the two-phase model. This partly can be explained by that the calibration of $k_{L,i}$ and a_i rely on parameters, i.e., d_b, V_r, ε_G, of which the estimation currently represent major knowledge gaps in literature. For example, the bubble characteristics – i.e., shape, size distribution and terminal velocity using surface aeration – are not well understood. To overcome this, previous studies, employing 2-phase models (e.g., Matko et al., 2021) use calibration methods that rely on fine-bubble aeration model parameter. This calibration practice can yield sufficient predictive accuracy in terms of oxygen mass-balances and dissolved concentration using SOTE values, in addition to d_b. In contrast, the prediction of N_2O gas mass transfer are not directly impacted by SOTE – but by the $k_{L,O2}$ and a_{O2} values (Eq. (2)), which renders model parameter tuning exercises limited to only d_b. As demonstrated here, this is insufficient to achieve accurate prediction of both DO and N_2O gas mass-transfers. This knowledge gap renders 2-phase models presently unsuitable to predict N_2O greenhouse gas emission from surface aerated reactors. As a result, parameter sensitivity and regression meta-model identification are carried out using single-phase simulation models in this contribution.

4.2. Clean water test simulations

Single-phase CFD simulation results predict currents with high oxygen concentration to only penetrate to a maximum depth of ~1 metre beneath the liquid surface, after which the current resurfaces (Fig. 7a). Two regions in the reactor volume – i.e. surface and sub-surface layers – are distinguished in the computational domain, in which gas-liquid mass transfer processes are modelled differently. First, values of $K_La_{O2,clean}$ were calculated using computed oxygen profiles obtained in the monitoring spatial Points 1–5 (Fig. 4a), located in the surface layer, and by plotting $\ln\left(\frac{S_O^*}{S_O^* - S_O}\right)$ against time (Fig. 7b).

$K_La_{O2,clean}$ values obtained in the reactor surface and in the water layer underneath (Fig. 7a) were plotted as a function of their distance from the rotor (Fig. 7c and d, respectively). Correlation equations for

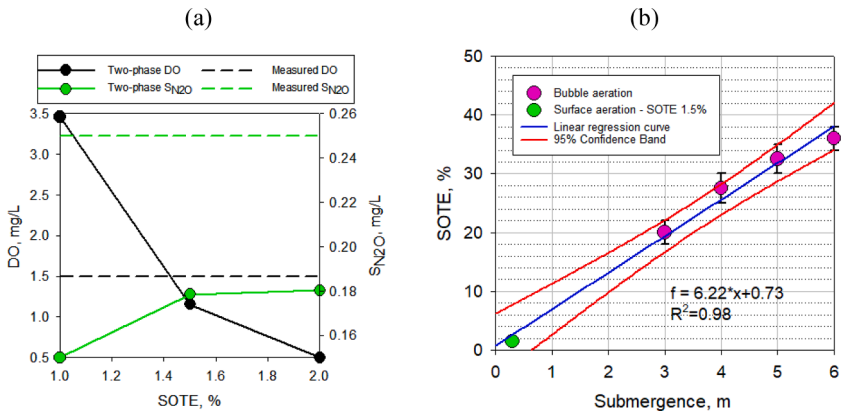

Fig. 5. (a) SOTE calibration with two-phase model and (b) linear regression equation between SOTE and aerator submergence. The bubble aeration data are from (Xylem, 2022).

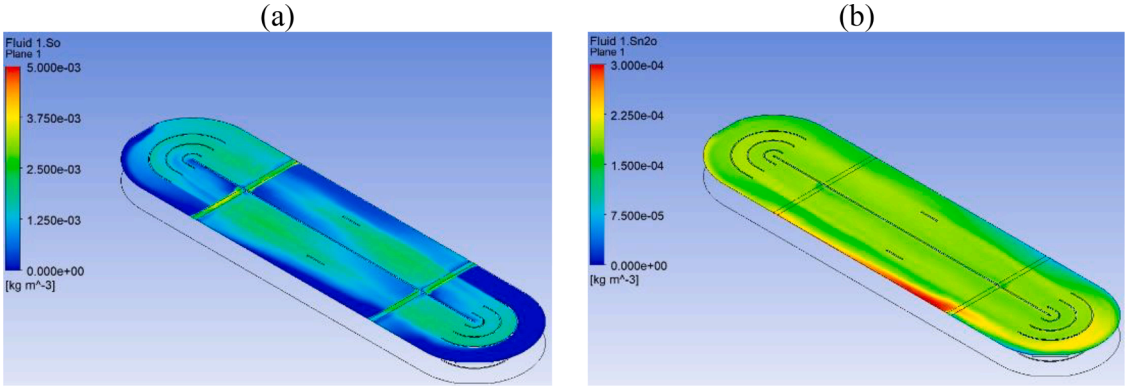

Fig. 6. Two-phase CFD simulation results obtained for dissolved oxygen (a) and N2O concentration (b) fields (SOTE=1.5 %, Fig. 8).

values of $K_La_{O2,clean}$ and the spatial distance to the rotor – for the two different reactor volume layers – were identified using logarithmic and constant (Fig. 7 and Table S7 for 16 screening tests) functions for the surface and sub-surface layers, respectively, and were then used for the Lynetten WRRF reactor simulations (Fig. 9).

$K_La_{O2,clean}$ values obtained in the reactor surface were used to estimate the α factor in the Lynetten WRRF reactor basin (Fig. 8). This was done by first approximating the K_La_{N2O} values – calculated based on liquid N_2O sensor data obtained in the five monitoring points – by substituting $K_La_{O2,clean}$ values in Eq. (2). The best-fit for K_La_{N2O} (Fig. 8) was obtained at $\alpha = 0.38 \pm 0.18$. D. Rosso and Stenstrom (2014) had suggested that, with surface aeration, α value can reach 0.8–1 due to the higher Reynolds number ($\sim 8 \times 10^4$). Compared to literature, our α value is relatively low. This is because the oxidation ditch in Lynetten WRRF is a large and not well-mixed reactor, thus the Reynolds number is not the same in the whole tank. The averaged Reynolds number in the simulation model is around 1×10^4, which can explain the lower average α value. Moreover, the highest discrepancy between the fitted and measured K_La_{N2O} values (Fig. 8) are those measured the nearest to the surface rotor characterised with advective interfacial flow transport regime. Noteworthy is that such flow conditions can increase locally the α factor that can cause spatially varying α factor values in real systems (Rosso and Stenstrom, 2006; D. 2014). As a practical approach, to simulate the measured DO and N_2O liquid concentration in the Lynetten WRRF (Fig. 9), the α factor is set to 0.38 [-].

4.3. Simulation of measured oxygen and N_2O data in Lynetten WRRF

4.3.1. Single-phase model

The average simulated DO and N_2O concentrations at the liquid surface are obtained at around 1.6 mg/L and 0.25 mg/L, respectively (Fig. 9c and d). These values closely agree with the measured data obtained under aerated operational phases with oxygen concentration, $S_O>0$ (Fig. 9a). We note that, using the un-refined mesh, the average DO and N_2O concentration data – 4.8 and 0.265 mg L^{-1}, respectively – show significant error introduced, in particular, in the predicted DO concentration (Fig. S5), thus indicating the benefits of adhering to good modelling practice in setting up CFD models.

As for the sensor data, in contrast to the CFD simulations – carried out under continuous surface aeration – the monitoring of the system involved multiple aeration periods. The average CFD simulation results (see red line in Fig. 9a) obtained for DO concentration show close agreement with the measured data. Similarly, the simulated average liquid N_2O concentration in the liquid surface can effectively predict the measured data (Fig. 9b).

The N_2O emission factor normalized to the total influent nitrogen in Lynetten is obtained around 0.69 %. According to Kampschreur et al. (2009) report on the N_2O emission factor from full scale activated sludge reactor, ranging from 0 to 14.6 % with an avereage of 0.6 % rate.

4.4. Factorial screening study

Screening of design and operational boundary conditions and their relative sensitivity to predict gas mass-transfer is done by setting up 16

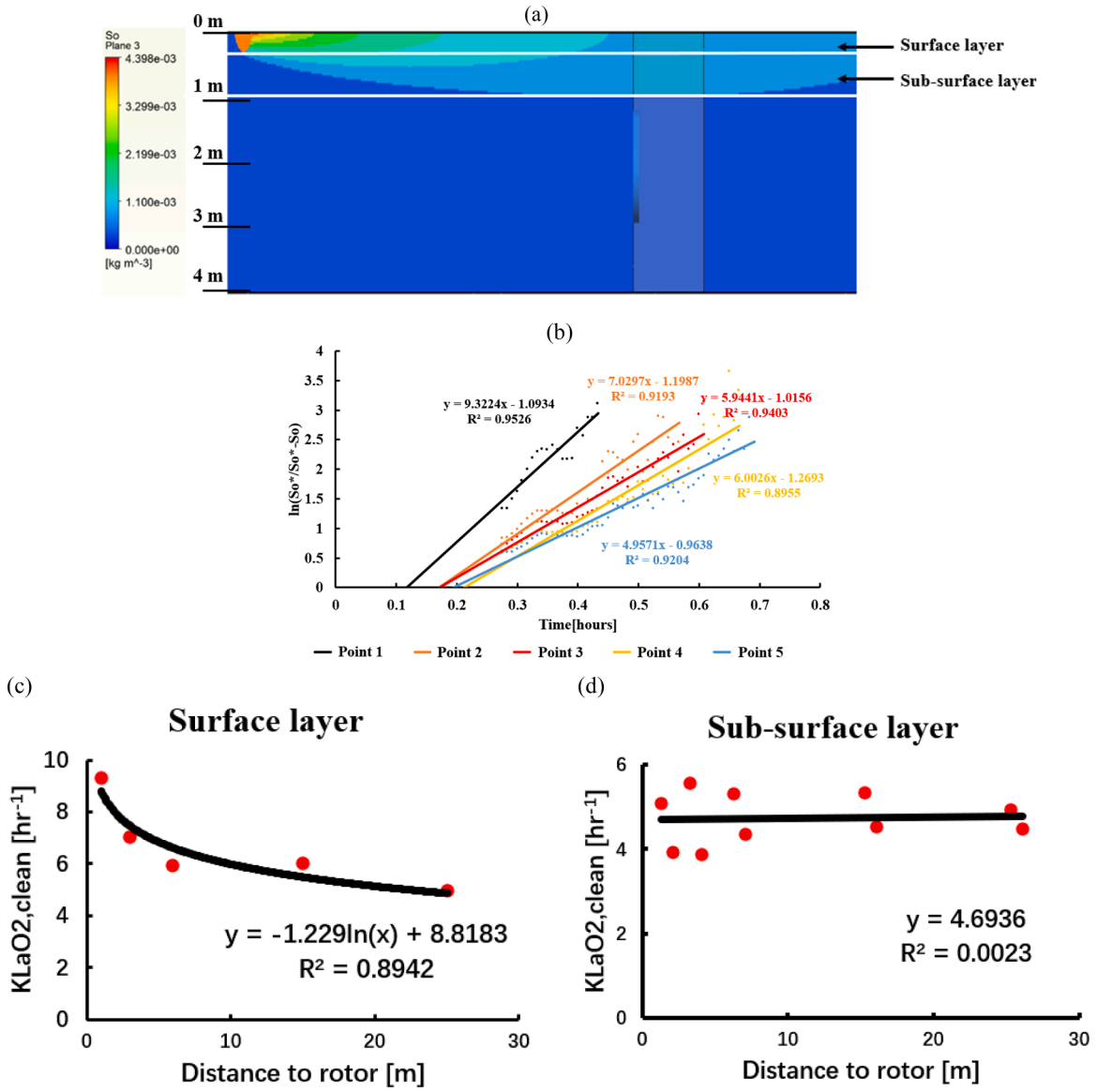

Fig. 7. Clean water gas mass-transfer results to evaluate the spatial variation of clean water KLa (*KLaO2,clean*). Simulated DO concentration for one rotors in a clean water test (a). Estimation of KLa values obtained for one of the rotors in the clean water test of the Lynetten WRRF reactor using normalized dissolved oxygen concentration values plotted against computational time elapsed (b). Spatial variation of oxygen gas mass-transfer coefficients in the surface aerated oxidation ditch reactor and regression analysis for *KLaO2,clean* as a function of distance to the rotor surface layer (c) and sub-surface layer (d). The thickness of the surface and subsurface layers are 0.3 m and 0.7 m, respectively. Note: in Fig. 4a, the propeller installed in the tank is additionally featured.

simulations based on the principles of the design of experiments method. The reactor design and operational parameter ranges, the predicted $K_La_{O2,clean}$ values in 15 monitoring points, as well as the regression equations predicting the $K_La_{O2,clean}$ field spatially in the surface and sub-surface layers are shown in the SI (Table S7). The K_La_{N2O} field is calculated in the computational domain by substituting $K_La_{O2,clean}$ values in Eq. (2).

Outputs obtained in the factorial screening are used to infer standardized multi-component polynomial regression equations for $K_La_{O2,clean}$ in both surface and sub-surface layers as a function of design and reactor operating conditions as

$$K_La_{O2,\ clean,\ surface} = 1.348\ \times \omega_{rotor} + 0.417\ \times T + 4.518 \quad (20)$$

$$K_La_{O2,\ clean,\ sub-surface} = 0.925\ \times \omega_{rotor} + 0.876\ \times T - 0.333\ \times \frac{L}{D} + 5.134 \quad (21)$$

where ω_{rotor} represents rotor speed, T denotes liquid temperature and L/D represents reactor length-to-depth ratio.

The relative slope values (b_i) in the linear polynomials (Eqs. (20) & (21)), allow the assessment of the relative sensitivity of parameters to predict the $K_La_{O2,clean}$ field. For both surface and sub-surface layers, rotor speed was obtained as the most dominant parameter, i.e. b_w exhibits the highest absolute value; its value is positive that can be explained by the fact that as the higher the rotor speed is, the higher the fluid velocity and thus increased efficiency of gas-liquid mass transfer achieved is. The relative slope value for liquid temperature was the second highest. Its value is positive, as expected based on thermodynamics (Arrhenius coefficient, $\theta = 1.024$) thus indicating that, with increasing temperature, values of $K_La_{O2,clean}$ increases. The L/D ratio – the third most important parameter according to its respective slope value – and any increase thereof can decrease $K_La_{O2,clean}$ in the sub-surface layer – which is not the case for the surface layer. The longer the reactor, the less effective the gas-liquid mass transfer in the sub-surface water volume, on average, will be, as a result of currents with

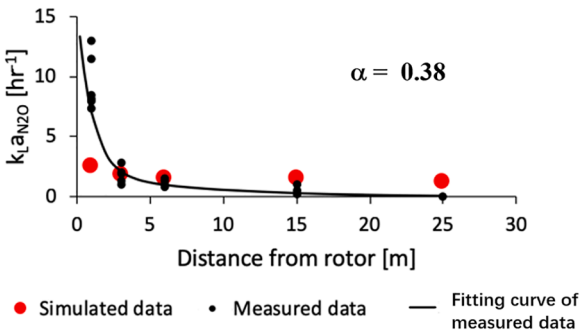

Fig. 8. Estimation of the α factor in the Lynetten WRRF reactor basin – by approximating the measured *KLaN2O* values (full-scale hood measurements – black dots connected with solid line) using the estimated spatially varying *KLaO2,clean* values in Eq. 2. α = 0.38 ± 0.18. Note: solid black line indicates the trendline fitted on the measured data to improve the understanding of the figure.

high oxygen concentration only penetrating a maximum depth of ~1 metre beneath the liquid surface, after which they resurface.

For clarity, spatial calibration of $K_La_{O2,clean}$ involves non-linear and constant functions implemented in a near-to-liquid surface and sub-surface layers in the computational domain, respectively (Fig. 5c and d). Conversely, a polynomial function is obtained from the subsequent factorial screening, employing the outputs of the calibrated simulation model, predicting, notably, N_2O liquid–gas mass transfer.

To be able to compare sensitivity results obtained on N_2O emission with data from literature (Domingo-Felez et al., 2019), absolute values of standardised b_i values are shown in Fig. 10. Additionally, in the polynomial regression function (Eq. (22)), slope values indicate whether a factor has negative or positive effect on N_2O emission.

The standardized multi-component polynomial regression equation obtained in the screening study for the predicted N_2O emission is as

$$N_2O\ emission = -0.212 \times L_{NH,Inf} - 0.091 \times T - 0.067 \times X_{tot} + 0.061 \times \mu_{AOB,\ HAO} + 0.047 \times \omega_{rotor} + 0.045 \times \mu_{NOB} - 0.041 \times COD/N + 0.482 \quad (22)$$

where N_2O eimission rate percentage calculated as a function of influent free and saline ammonia–nitrogen concentration, COD/N ratio is the ratio between chemical oxygen demand and nitrogen, $L_{NH,Inf}$ is ammonia loading, X_{tot} is total biomass concentration in the reactor, ω_{rotor}

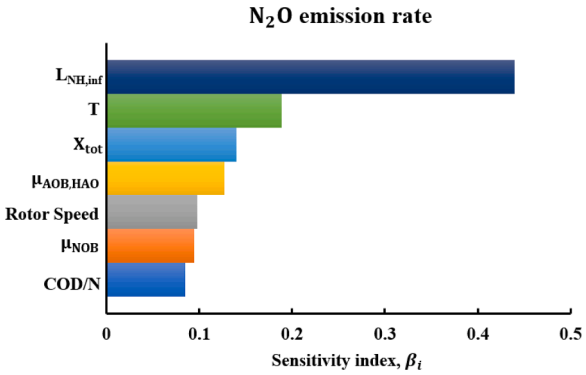

Fig. 10. Sensitivity indices standardised to the intercept value (in Eq. 22) obtained the factorial screening experiment for N2O emission factor. Note: intercept value in Eq. 22 equals 0.482.

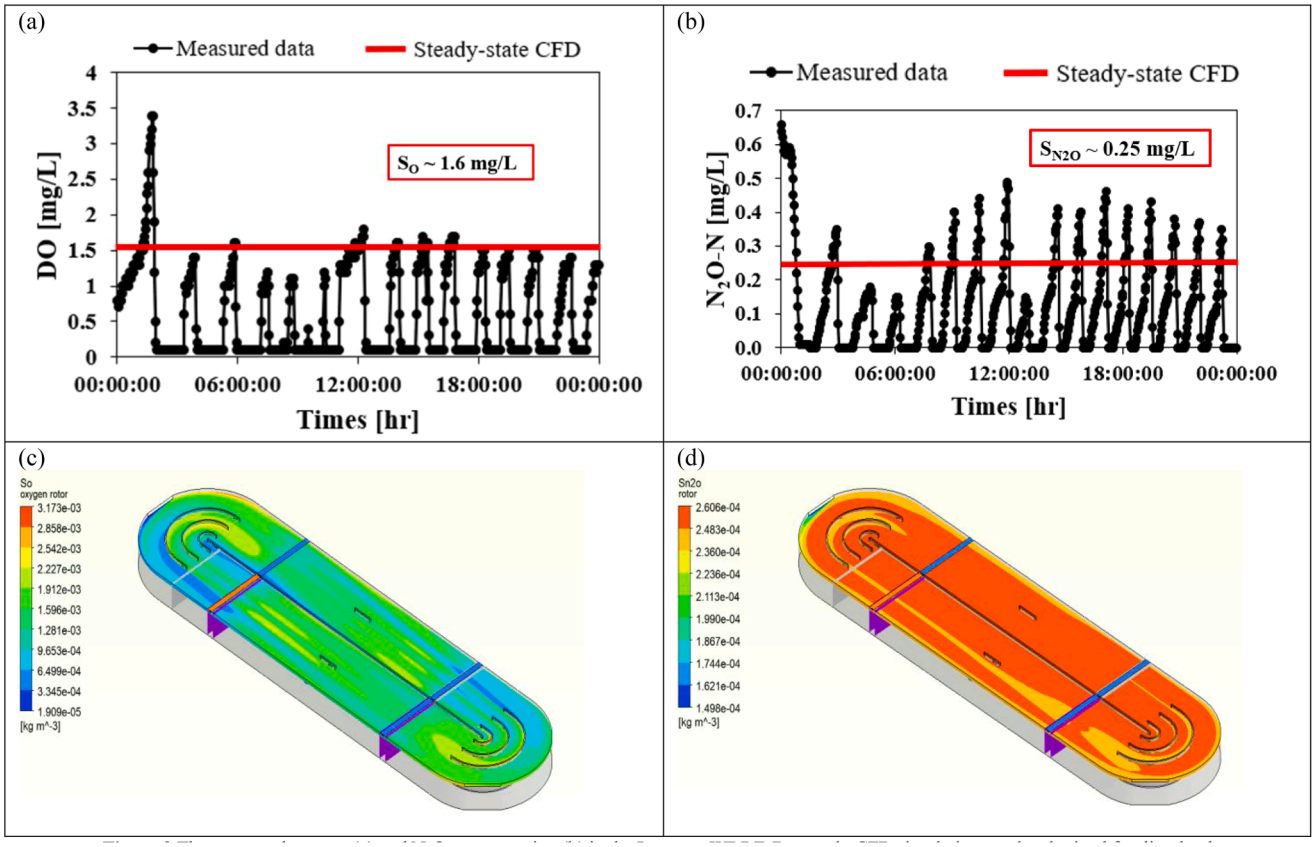

Fig. 9. The measured oxygen (a) and N2O concentration (b) in the Lynetten WRRF, Denmark, CFD simulation results obtained for dissolved oxygen (c) and N2O concentration (d) field.

represents rotor speed, T denotes temperature, μ_{NOB} is aerobic NOB specific growth rate and $\mu_{AOB,\ HAO}$ is maximum specific growth rate for NH_2OH oxidation. The design and operating parameters in Eq. (22) are between +1/−1, and therefore the b_i indices are unitless.

Sensitivity analysis results (Fig. 10) – obtained as the slope values standardised by the intercept value shown in Eq. (22) – show that N_2O emission is most impacted by the ammonia loading ($L_{NH,Inf}$). The negative impact of $L_{NH,Inf}$ (Eq. (22)) can be explained by the fact that the lower ammonia loading will allow less N_2O to form biologically and thus less N_2O to be stripped from the liquid phase. Liquid temperature was obtained as the second important parameter; its negative sensitivity index that can be explained by the fact that lower liquid temperature can increase the production rate of nitrite, and the higher nitrite concentration can lead to increased N_2O emission (Kampschreur et al., 2009). Regarding Eqs. (20)–(21), positive sensitivity for $K_La_{O2,clean}$ implies that liquid temperature can increase N_2O gas–liquid mass transfer (Eq. (2)), and thus on N_2O emission. The negative impact of biokinetic processes on N_2O emission, however, seems to more than just compensate for the positive impact of liquid temperature, thus resulting in an overall negative sensitivity index value. The negative sensitivity of X_{tot} suggests that the higher the biomass concentration in the reactor, the higher the overall biokinetic conversion rates are that can potentially reduce N_2O production and thus emission factors. The next parameter in the significance ranking (Fig. 8) is $\mu_{AOB,\ HAO}$; the positive impact of this parameter on N_2O emission is because the higher the specific AOB growth rate is the more enhanced the oxidation of NH_2OH is, thereby increasing the N_2O production and emission. The higher rotor speed can lead to higher oxygen mass transfer coefficient and then increase the stripping of N_2O (Kampschreur et al., 2009), which is why the rotor speed has positive impact to the N_2O emission.

The $b_{m\text{-}NOB}$ sensitivity index is a positive value, which can be explained by that the higher its value, the higher the denitrification rate of HNO_2 to N_2O will be. Additionally, Kampschreur et al. (2009) suggest that lower COD/N ratio can increase N_2O emission during denitrification, that agrees with our parameter sensitivity results, i.e. $b_{COD/N}$ for COD/N.

(Domingo-Félez et al., 2017) present global sensitivity analysis results on biokinetic parameters, including absolute values of b_i. To predict N_2O concentration in a sequencing batch reactor (SBR) using synthetic wastewater, their results indicate $\mu_{AOB,\ HAO}$ as one of the most influential parameter amongst biokinetic and stoichiometric parameters in the NDHA model – 5th in the ranking. Taken together, design- and operational boundary conditions are found equally or even more important than biokinetic parameters to enhance N_2O emission from surface aerated activated sludge reactors.

4.5. Calibration of $K_La_{O2,clean}$ and N_2O emission factors using polynomial regression equations

Besides local sensitivity by means of factor screening, polynomial regression equations can also be converted into regression meta-models. Inferring such algebraic predictors of $K_La_{O2,clean}$ and N_2O emission factor is useful for practitioners to calibrate gas–liquid mass transfer models and to approximate greenhouse gas emission, respectively, in e.g., WRRF plant-wide simulation models.

To predict gas-mass transfer in surface-aerated activated sludge reactors using data-driven meta-models, outputs obtained in the factorial screening study were used to infer the non-standardized multi-component polynomial regression equations for $K_La_{O2,clean}$ in both surface and sub-surface layers as a function of design and reactor operating conditions as

$$K_La_{O2,\ clean,\ surface} = 0.039\ \times \omega_{rotor} + 0.083\ \times T + 2.055 \quad (23)$$

$$K_La_{O2,\ clean,\ sub-surface} = 0.026\ \times \omega_{rotor} + 0.175\ \times T - 0.033\ \times L/D + 2.686 \quad (24)$$

where ω_{rotor} represents rotor speed [rpm], T denotes temperature [°C] and L/D represents reactor length-to-depth ratio [-].

Predictions obtained with Eqs. (23) and 24 were benchmarked against the $K_La_{O2,clean}$ values obtained in the 15 monitoring points in the clean-water CFD simulations (Fig. 11); results indicate close agreement in both surface and sub-surface water layers.

The meta-model for N_2O emission is obtained as

$$N_2O\ emission = -0.0002\ \times L_{NH,Inf} - 0.0182\ \times T - 4.497\ \times 10^{-5} \times X_{tot} + 0.3142\ \times \mu_{AOB,\ HAO} + 0.0014\ \times \omega_{rotor} + 0.1748\ \times \mu_{NOB} - 0.0086\ \times COD/N + 0.8849 \quad (25)$$

where N_2O eimission factor percentage calculated as a function of influent free and saline ammonia-nitrogen concentration, COD/N ratio is the ratio between chemical oxygen demand and nitrogen [-], $L_{NH,Inf}$ is ammonia loading [kgN d^{-1}], X_{tot} is total biomass concentration in the reactor [mg L^{-1}], ω_{rotor} represents rotor speed [rpm], T denotes temperature [°C], μ_{NOB} is aerobic NOB specific growth rate [d^{-1}] and $\mu_{AOB,\ HAO}$ is maximum specific growth rate for NH_2OH oxidation [d^{-1}].

N_2O emission values predicted using Eq. (25) show close agreement with values predicted by the CFD simulation model using the 16 different design and operational boundary conditions, thus validating the N_2O emission predictors (Fig. 12). We note that, in the absence of a WRRF simulation model, Eq. (25) can offer practitioners a tool to predict greenhouse gas emission from full-scale WRRF as a function of $L_{NH,Inf}$.

5. Outlook and perspective

To calibrate 2-phase CFD simulation models for mechanical surface aeration, effective prediction of bubble size distribution (BSD) is critical to estimate a_i - similar to that for fine bubble aeration (Amaral et al., 2018). Presently, there is a lack of understanding of bubble characteristics in SASR that renders the estimation of a_i challenging – a hinderance to predictive accuracy as demonstrated in this contribution. That is, bubble coalescence has a significant impact on gas mass-transfer processes – with minimal influence of the initial bubble sizes on the overall mass transferred as compared to the SOTE. To account for bubble coalescence and break up Population Balance Models (PBM) can be implemented (Ding et al., 2006; Climent et al., 2019). However, PBMs include a set of additional parameters – e.g., volume fraction of different bubble sizes, mass birth/death rate for bubble coalescence and break up that are not straightforward to calibrate (Alhendal et al., 2019; Climent et al., 2019). Furthermore, different rotor geometries, submergence and rotation speed can affect bubble characteristics – also less-well understood in literature (Huang et al., 2009; Qiu et al., 2018) –thus, requiring BSD to be re-computed every time when adjusting the rotor operation. In SASR, the bubble density remains small and its interaction with the flow is limited to regions close to the surface (Fan et al., 2010) and near to the surface aeration rotors. Consequently, there is little influence by bubbles generated on the liquid flow in the reactor – as opposed to fine-bubble aeration. With respect to the bubble distribution, one can expect significant coalescence and break-up given the huge amount of air entrapped by the paddles. The resulting bubble sizes therefore are hypothesised to be dependent on the balance between coalescence and break-up in the vicinity of the rotors.

In 2-phase simulation models, there is an oxygen transfer rate defined for the surface aerator boundary condition (K_La_{BC}·V) with V denoting the reactor volume. In literature, the estimation of K_La_{BC} is based on assumptions that rely on e.g., single K_La values for a type of rotor that ignores the impact of rotor speed and/or rotor immersion (Guo et al., 2020; Thakre et al., 2008). These practices can introduce considerable uncertainties in simulations – an area the present contribution aims to amend by providing more systematic calibration practices.

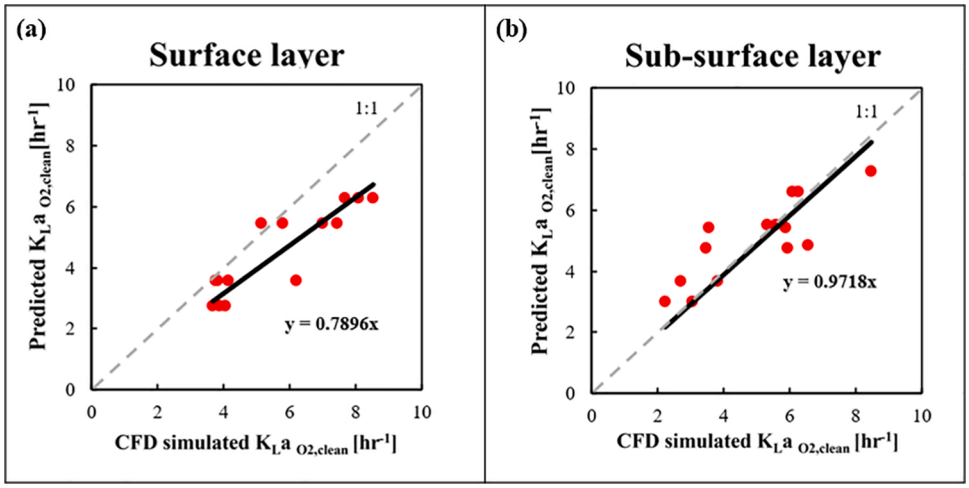

Fig. 11. Predicted values of (a) spatial averaged *KLaO2,clean* in the surface layer and (b) sub-surface layer using regression equations as a function of values predicted using CFD simulation model.

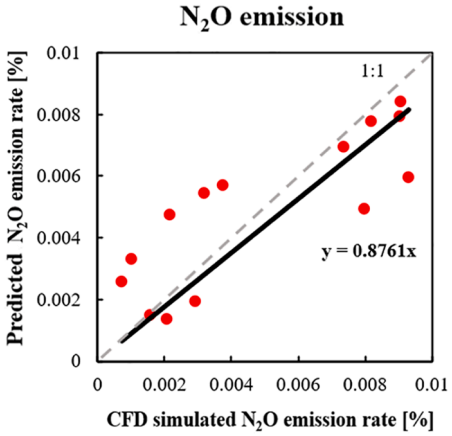

Fig. 12. Validation of the meta-model (Eq. 25) using CFD simulation results obtained with the 16 reactor design meshes and operational conditions.

Additionally, for surface aeration systems, the source term for the gas phase is proposed as a major knowledge gap in literature to be investigated. We recommend these efforts to be directed towards a complete description of the spatial distribution of the air bubbles generated in the domain and the bubble sizes at every location. From laboratory experiments with reduced scale rotors (data not shown), it is apparent that the air bubbles are generated by two different phenomena. On the one hand, there is a direct contribution caused by air entrapped by the rotating paddles. On the other hand, there is an indirect contribution caused by the drops that are splashed out when the paddles emerge from the water. These drops entrap air then they fall again onto the water surface, generating bubbles beyond the region where the rotors are located. These two phenomena lead to two different spatial distributions of bubbles, as well as to two different bubble size distributions. Both distributions depend on the size of the paddles, the rotor submergence and its rotational speed. To sum up, the multiphase characterization of rotors is an extremely complex task that should be specifically studied in future works.

6. Conclusion

The following concluding remarks are drawn:

- A calibration protocol for single- and two-phase CFD simulation models – accounting for biokinetic and physical-chemical hydrodynamics – of surface aerated oxidation ditch-type reactors is presented.
- The two-phase surface aerator model, whilst it can capture the most relevant multiphase phenomena, can't presently be used to reliably predict aeration and N_2O emission in tandem. To achieve that, further research is necessary to extend the state-of-the-art, notably, by improving our understanding of bubble size distribution.
- A new method of estimating the average alpha factor using hood measurement data in the WRRF Lynetten full-scale reactor system is presented.
- The calibrated single-phase CFD model is validated against full-scale measurement data from Lynetten WRRF, Denmark.
- Results obtained in a factor screening (local sensitivity) study show that the prediction of $K_La_{O2,clean}$ is influenced by rotor speed, temperature and L/D ratio. Additionally, N_2O emission is shown to be influenced by parameters Q_{in}, temperature, X_{tot}, $\mu_{AOB,\ HAO}$, ω_{rotor}, μ_{NOB} and COD/N ratio.
- Predictors for $K_La_{O2,clean}$ and N_2O emissions by means of linear polynomial regression functions have been inferred as a function of important design and operating parameters. The function can be useful to calibrate simpler zero- and one-dimensional distributed reactors models.

CRediT authorship contribution statement

Yuge Qiu: Data curation, Formal analysis, Funding acquisition, Methodology, Software, Validation, Writing – original draft, Visualization. **Sara Ekström:** Data curation. **Borja Valverde-Pérez:** Supervision. **Barth F. Smets:** Supervision. **Javier Climent:** Methodology, Software. **Carlos Domingo-Félez:** Methodology. **Raúl Martínez Cuenca:** Methodology, Software. **Benedek G. Plósz:** Conceptualization, Project administration, Supervision, Writing – review & editing.

Declaration of competing interest

The authors declare that they have no known competing financial interests or personal relationships that could have appeared to influence the work reported in this paper.

Data availability

Data will be made available on request.

Acknowledgments

This research was partially funded by the Danish Agency for Science, Technology and Innovation through the Research Project LaGas (12-132633). We are grateful to Christopher T. Griffin who was part of this project at an early stage, and who contributed to the setup of the CFD simulation platform. We would like to thank Carsten Thirsing, BIOFOS, the operator of Lynetten WRRF for all the help and support of our field experimental work. The authors have no conflict of interest to declare. We acknowledge the generous support of Mr. Yichen Qiu and Mrs. Pingyun Ge, parents of Ms. Yuge Qiu (first author), and their financial support received.

Supplementary materials

Supplementary material associated with this article can be found, in the online version, at doi:10.1016/j.watres.2024.121398.

References

Alhendal, Y., Turan, A., Kalendar, A., Abou-Ziyan, H., 2019. Bubble population balance modelling for stationary and rotating columns under zero-gravity environment: numerical study. Adv. Mech. Eng. 11 (10), 11–13. https://doi.org/10.1177/1687814019885259.

Amaral, A., Schraa, O., Rieger, L., Gillot, S., Fayolle, Y., Bellandi, G., Amerlinck, Y., Mortier, S.T.F.C., Gori, R., Neves, R., Nopens, I., 2017. Towards advanced aeration modelling: from blower to bubbles to bulk. Water Sci. Technol. 75 (3), 507–517.

Amaral, A., Bellandi, G., Rehman, U., Neves, R., Amerlinck, Y., Nopens, I., 2018. Towards improved accuracy in modeling aeration efficiency through understanding bubble size distribution dynamics. Water Res. 131, 346–355.

APHA, 1999. Standard Methods for the Examination of Water and Wastewater, 20th ed. American Public Health Association, Washington DC, US.

Baker, N., Kelly, G., O'Sullivan, P.D., 2020. A grid convergence index study of mesh style effect on the accuracy of the numerical results for an indoor airflow profile. Int. J. Vent. 19 (4), 300–314. https://doi.org/10.1080/14733315.2019.1667558.

Bencsik, D., Takács, I., Rosso, D., 2022. Dynamic alpha factors: prediction in time and evolution along reactors. Water Res. 216, 118339 https://doi.org/10.1016/j.watres.2022.118339.

Climent, J., Martínez-Cuenca, R., Carratalà, P., González-Ortega, M.J., Abellán, M., Monrós, G., Chiva, S., 2019. A comprehensive hydrodynamic analysis of a full-scale oxidation ditch using population balance modelling in CFD simulation. Chem. Eng. J. 374, 760–775. https://doi.org/10.1016/j.cej.2019.05.195.

Cumby, T.R., 1987. A review of slurry aeration 3. Performance of aerators. J. Agric. Eng. Res. 1987 (36), 175–206. https://doi.org/10.1016/0021-8634(87)90073-4.

Deacon, E.L., 1977. Gas transfer to and across an air-water interface. Tellus 29 (4), 363–374. https://doi.org/10.3402/tellusa.v29i4.11368.

Ding, A., Hounslow, M.J., Biggs, C.A., 2006. Population balance modelling of activated sludge flocculation: investigating the size dependence of aggregation, breakage and collision efficiency. Chem. Eng. Sci. 61, 63–74. https://doi.org/10.1016/j.ces.2005.02.074.

Domingo-Félez, C., Calderó-Pascual, M., Plósz, B.G., Smets, B.F., Sin, G., 2017. Calibration of the comprehensive NDHA-N2O dynamics model for nitrifier-enriched biomass using targeted respirometric assays. Water Res. 126, 29–39. https://doi.org/10.1016/j.watres.2017.09.013.

Domingo-Félez, C., Mutlu, A.G., Jensen, M.M., Smets, B.F., 2014. Aeration strategies to mitigate nitrous oxide emissions from single-stage nitritation/anammox reactors. Environ. Sci. Technol. 48, 8679–8687. https://doi.org/10.1021/es501819n.

Domingo-Félez, C., Smets, B.F., 2016. A consilience model to describe N_2O production during biological N removal. Environ. Sci. Water Res. Technol. 2, 923–930. https://doi.org/10.1039/c6ew00179c.

Domingo-Félez, C., Smets, B.F., 2020. Modelling N_2O dynamics of activated sludge biomass: uncertainty analysis and pathway contributions. Chem. Eng. J. 379, 122311 https://doi.org/10.1016/j.cej.2019.122311.

Fan, L., Xu, N., Wang, Z., Shi, H., 2010. PDA experiments and CFD simulation of a lab-scale oxidation ditch with surface aerators. Chem. Eng. Res. Des. 88, 23–33. https://doi.org/10.1016/j.cherd.2009.07.013.

Gostelow, P., Parsons, S.A., Cobb, J., 2001. Development of an adorant emission model for sewage treatment works. Water Sci. Technol. 44 (9), 181–188. https://doi.org/10.2166/wst.2001.0535.

Guo, J., Dong, L., Liu, J., 2020. Numerical simulation of the gas-liquid two-phase flow in aeration tank based on different multiphase models. J. Phys.: Conf. Ser. 1600 (1), 012084 https://doi.org/10.1088/1742-6596/1600/1/012084.

Guyonvarch, E., Ramin, E., Kulahci, M., Plósz, B.G., 2015. iCFD: interpreted computational fluid dynamics - degeneration of CFD to one-dimensional advection-dispersion models using statistical experimental design - The secondary clarifier. Water Res. 83, 396–411. https://doi.org/10.1016/j.watres.2015.06.012.

Guyonvarch, E., Ramin, E., Kulahci, M., Plósz, B.G., 2020. Quantifying the sources of uncertainty when calculating the limiting flux in secondary settling tanks using iCFD. Water Sci. Technol. 81, 241–252. https://doi.org/10.2166/wst.2020.090.

Hemrajani, R.R., Tatterson, G.B., 2004. Mechanically Stirred Vessels, in: handbook of Industrial Mixing. https://doi.org/10.1002/0471451452.ch6.

Hibiki, T., Ishii, M., 2011. Thermo-fluid Dynamics of Two-Phase Flow. Springer, London.

Huang, W., Wu, C., Xia, W., 2009. Oxygen transfer in high-speed surface aeration tank for wastewater treatment: full-scale test and numerical modeling. J. Environ. Eng. 135 (8), 684–691. https://doi.org/10.1061/(asce)ee.1943-7870.0000023.

Huang, W., Li, K., Wang, G., Wang, Y., 2013. Computational fluid dynamics simulation of flows in an oxidation ditch driven by a new surface aerator. Environ. Eng. Sci. 30 (11), 663–671. https://doi.org/10.1089/ees.2012.0313.

Huang, J., Qu, X., Wan, M., Ying, J., Li, Y., Zhu, F., Wang, J., Shen, G., Chen, J., Li, W., 2015. Investigation on the performance of raceway ponds with internal structures by the means of CFD simulations and experiments. Algal Res. 10, 64-71.

ICF, 2019. User's Guide for Estimating Carbon dioxide, methane, and Nitrous Oxide Emissions from Agriculture Using the State Inventory Tool [WWW Document]. URL. https://www.epa.gov/sites/default/files/2017-12/documents/ag_module_users_guide.pdf. accessed 25/11/21.

Sack, J.-R, Urrutia, J., 2008. Handbook of Computational Geometry. Elsevier, Amsterdam Etc.

Kampschreur, M.J., Temmink, H., Kleerebezem, R., Jetten, M.S.M., van Loosdrecht, M.C.M., 2009. Nitrous oxide emission during wastewater treatment. Water Res. 43 (17), 4093–4103. https://doi.org/10.1016/j.watres.2009.03.001.

Kampschreur, M.J., van der Star, W.R.L., Wielders, H.A., Mulder, J.W., Jetten, M.S.M., van Loosdrecht, M.C.M., 2008. Dynamics of nitric oxide and nitrous oxide emission during full-scale reject water treatment. Water Res. 42 (3), 812–826. https://doi.org/10.1016/j.watres.2007.08.022.

Karpinska, A.M., Bridgeman, J., 2016. CFD-aided modelling of activated sludge systems - a critical review. Water Res. 88 (1), 861–879. https://doi.org/10.1016/j.watres.2015.11.008.

Le Moullec, Y., Gentric, C., Potier, O., Leclerc, J.P., 2010. CFD simulation of the hydrodynamics and reactions in an activated sludge channel reactor of wastewater treatment. Chem. Eng. Sci. 65, 492–498. https://doi.org/10.1016/j.ces.2009.03.021.

Luo, H., Svendsen, H.F., 1996. Theoretical model for drop and bubble breakup in turbulent dispersions. AIChE J. 42, 1225–1233. https://doi.org/10.1002/aic.690420505.

Mackay, D., Yeun, A.T.K., 1983. Mass transfer coefficient correlations for volatilization of organic solutes from water. Environ. Sci. Technol. 17 (4), 211–217. https://doi.org/10.1021/es00110a006.

Matko, T., Chew, J., Wenk, J., Chang, J., Hofman, J., 2021. Computational fluid dynamics simulation of two-phase flow and dissolved oxygen in a wastewater treatment oxidation ditch. Process Saf. Environ. Prot. 145, 340–353. https://doi.org/10.1016/j.psep.2020.08.017.

Menter, F.R., 1993. Zonal two equation κ-ω turbulence models for aerodynamic flows. In: AIAA 23rd Fluid Dynamics, Plasmadynamics, and Lasers Conference, 1993.

Menter, F.R., 2009. Review of the shear-stress transport turbulence model experience from an industrial perspective. Int. J. Comut. Fluid Dyn. 23, 305–316. https://doi.org/10.1080/10618560902773387.

Mueller, J.A., Boyle, W.C., Pöpel, H.J., 2002. Aeration: principles and practice, Aeration: principles and Practice.

Murthy, S., Jayanti, S., 2002. CFD study of power and mixing time for paddle mixing in unbaffled vessels. Chem. Eng. Res. Des. 80 (5), 482–498. https://doi.org/10.1205/026387602320224067.

Ni, B.J., Peng, L., Law, Y., Guo, J., Yuan, Z., 2014. Modeling of nitrous oxide production by autotrophic ammonia-oxidizing bacteria with multiple production pathways. Environ. Sci. Technol. 48 (7), 3916–3924. https://doi.org/10.1021/es405592h.

Ni, B.J., Yuan, Z., Chandran, K., Vanrolleghem, P.A., Murthy, S., 2013. Evaluating four mathematical models for nitrous oxide production by autotrophic ammonia-oxidizing bacteria. Biotechnol. Bioeng. 110 (1), 153–163. https://doi.org/10.1002/bit.24620.

Niño, L., Gelves, R., Ali, H., Solsvik, J., Jakobsen, H., 2020. Applicability of a modified breakage and coalescence model based on the complete turbulence spectrum concept for CFD simulation of gas-liquid mass transfer in a stirred tank reactor. Chem. Eng. Sci. 211, 115272 https://doi.org/10.1016/j.ces.2019.115272.

Plósz, B.G., Jobbágy, A., Grady, C.P.L., 2003. Factors influencing deterioration of denitrification by oxygen entering an anoxic reactor through the surface. Water Res. 37 (4), 853–863. https://doi.org/10.1016/S0043-1354(02)00445-1.

Pocquet, M., Wu, Z., Queinnec, I., Spérandio, M., 2016. A two pathway model for N_2O emissions by ammonium oxidizing bacteria supported by the NO/N_2O variation. Water Res. 88, 948–959. https://doi.org/10.1016/j.watres.2015.11.029.

Prata, A.A., Santos, J.M., Timchenko, V., Stuetz, R.M., 2018. A critical review on liquid-gas mass transfer models for estimating gaseous emissions from passive liquid surfaces in wastewater treatment plants. Water Res. 130, 388–406. https://doi.org/10.1016/j.watres.2017.12.001.

Prince, M.J., Blanch, H.W., 1990. Bubble coalescence and break-up in air-sparged bubble columns. AIChE J. 36, 1485–1499. https://doi.org/10.1002/aic.690361004.

Qiu, Y., Zhang, C., Li, B., Li, J., Zhang, X., Liu, Y., Liang, P., Huang, X., 2018. Optimal surface aeration control in full-scale oxidation ditches through energy consumption analysis. Water (Switzerland) 10 (7), 945. https://doi.org/10.3390/w10070945.

Ribera-Guardia, A., Bosch, L., Corominas, L., Pijuan, M., 2019. Nitrous oxide and methane emissions from a plug-flow full-scale bioreactor and assessment of its carbon footprint. J. Clean. Prod. 212, 162–172. https://doi.org/10.1016/j.jclepro.2018.11.286.

Roache, P.J., 1998. Verification of codes and calculations. AIAA J. 36 (5), 696–702. https://doi.org/10.2514/2.457.

Rosso, D., Stenstrom, M.K., 2014. Alpha factors in full-scale wastewater aeration systems. Proc. Water Environ. Fed. 2006 (7), 4853–4863. https://doi.org/10.2175/193864706783762940.

Rosso, D., Stenstrom, M.K., 2006. Surfactant effects on α-factors in aeration systems. Water Res. 40 (7), 1397–1404. https://doi.org/10.1016/j.watres.2006.01.044.

Schneider, M.Y., Quaghebeur, W., Borzooei, S., Froemelt, A., Li, F., Saagi, R., Wade, M.J., Zhu, J.-J., Torfs, E., 2022. Hybrid modelling of water resource recovery facilities: status and opportunities. Water Sci. Technol. 85, 2503–2524. https://doi.org/10.2166/wst.2022.115.

Stenstrom, M.K., Gilbert, R.G., 1981. Effects of alpha, beta and theta factor upon the design, specification and operation of aeration systems. Water Res. 15 (6), 643–654. https://doi.org/10.1016/0043-1354(81)90156-1.

Tchobanoglous, G., Burton, F.L., Stensel, H.D., 2003. Wastewater engineering : treatment and reuse. 4th ed. Metcalf & Eddy, Inc ; revised by G. Tchobanoglous, F.L. Burton, H. David Stensel, McGraw-Hill Series in Civil and Environmental Engineering.

Teshome, T.M., 2020. Computational Fluid Dynamics Application to Optimize and Evaluate the Performance of High Rate Algal Pond System (PhD Thesis). Université de, Strasbourg, France.

Tewari, P.K., Bewtra, J.K., 1982. Alpha and beta factors for domestic wastewater. J. Water Pollut. Control Fed. 54 (9), 1281–1287. https://www.jstor.org/stable/25041683.

Thakre, S., Bhuyar, L., Deshmukh, S., 2008. Effect of different configurations of mechanical aerators on oxygen transfer and aeration efficiency with respect to power consumption. Int. J. Aerosp. Mech 2 (2), 100–108. https://doi.org/10.5281/zenodo.1082237.

Tominaga, Y., Stathopoulos, T., 2007. Turbulent Schmidt numbers for CFD analysis with various types of flowfield. Atmos. Environ. 41 (37), 8091–8099. https://doi.org/10.1016/j.atmosenv.2007.06.054.

US EPA, 2001. User's Guide for WATER9 Software, 2nd ed [WWW Document]. URL https://www3.epa.gov/ttnchie1/software/water/water9/water9%20manual.pdf (Accessed 15 October 2021).

US EPA, 1994. Air Emission Models for Waste and Wastewater. North Carolina, USA [WWW Document]. URL https://www3.epa.gov/ttnchie1/software/water/air_emission_models_waste_wastewater.pdf (Accessed 15 October 2021).

Wicklein, E., Batstone, D.J., Ducoste, J., Laurent, J., Griborio, A., Wicks, J., Saunders, S., Samstag, R.W., Potier, O., Nopens, I., 2016. Good modelling practice in applying computational fluid dynamics for WWTP modelling. Water Sci. Technol. 73 (5), 969–982. https://doi.org/10.2166/wst.2015.565.

Wilcox, D.C., 1998. Turbulence Modeling For CFD, 2. DCW industries, La Canada, CA.

Xylem, 2022. Sanitaire ® Ceramic disc diffusers effective aeration for corrosive environments.

Zaburko, J., Głowienka, R., Widomski, M., Szulżyk-Cieplak, J., Babko, R., Łagód, G., 2020. Modeling of the aeration system of a sequencing batch reactor. J. Ecol. Eng. 21, 249–256. https://doi.org/10.12911/22998993/126240.